

Cite this: *RSC Adv.*, 2017, 7, 50663

# Reactive molecular dynamics study of the decomposition mechanism of the environmentally friendly insulating medium $C_3F_7CN$ †

Xiaoxing Zhang,<sup>a</sup> Yi Li,<sup>a</sup> Dachang Chen,<sup>a</sup> Song Xiao,<sup>\*a</sup> Shuangshuang Tian,<sup>a</sup> Ju Tang<sup>a</sup> and Ran Zhuo<sup>b</sup>

The extensive use of sulfur hexafluoride ( $SF_6$ ) gas in the power industry has a strong greenhouse effect. Hence, many scholars are committed to studying  $SF_6$  alternative gases to achieve green power development. In the past two years,  $C_3F_7CN$  (heptafluoroisobutyronitrile) has attracted the attention of many scholars due to its excellent insulation and environmental protection characteristics as a potential alternative gas. This study theoretically explores the decomposition characteristics of  $C_3F_7CN$  and the  $C_3F_7CN/CO_2$  gas mixture based on the reactive molecular dynamics method and density functional theory. The main decomposition pathways of  $C_3F_7CN$  and the enthalpy of each path at different temperatures were analyzed. The yield of the main decomposition products was obtained under several temperature conditions. The decomposition of  $C_3F_7CN$  mainly produced  $CF_3$ ,  $C_3F_7$ ,  $CN$ ,  $CNF$ ,  $CF_2$ ,  $CF$ ,  $F$ , and other free radicals and a few molecular products, such as  $CF_4$  and  $C_3F_8$ . The  $C_3F_7CN/CO_2$  gas mixture has more excellent decomposition characteristics than that of the pure  $C_3F_7CN$ . The addition of  $CO_2$  effectively ensures that the gas mixture has a low liquefaction temperature, which is considerably suitable for use as a gas insulation medium. The relevant research results provide guidance for the further exploration on the electrical properties and practical engineering application of the  $C_3F_7CN$  gas mixture.

Received 7th September 2017  
Accepted 18th October 2017

DOI: 10.1039/c7ra09959b

rsc.li/rsc-advances

## 1 Introduction

$SF_6$  (sulfur hexafluoride) is the most common insulation medium used in high-voltage (HV) electrical equipment such as gas insulated switchgear (GIS).<sup>1</sup> However,  $SF_6$  is a greenhouse gas (GHG) regulated under the Kyoto Protocol with a global warming potential (GWP) of 22 800.<sup>2,3</sup> Although the proportion of greenhouse effect caused by the use of  $SF_6$  is not as large as the amount of fossil fuel energy consumed, the global atmospheric content of  $SF_6$  has increased by 20% in the past five years and the atmospheric mole fraction of  $SF_6$  is 7.28 ppq currently corresponding to a radiative forcing of  $0.0041 \text{ W m}^{-2}$ .<sup>4,5</sup> The greenhouse effect has caused widespread public concern in recent years.<sup>6</sup> Climate deterioration caused by  $SF_6$  has gradually become one of the contradictions between power industry development and environmental protection. Hence, the power industry should gradually limit the use of  $SF_6$  and search for an

environmentally friendly alternative gas for  $SF_6$  in gas-insulated equipment.

$C_3F_7CN$  (heptafluoroisobutyronitrile) is a potential alternative gas for  $SF_6$  (see Fig. 1 for its molecular structure) with a GWP value of 2100 and Ozone Depression Potential (ODP) value of 0.4. The dielectric strength of  $C_3F_7CN$  is 2.74 times that of  $SF_6$ .<sup>7</sup> It should be used in combination with  $CO_2$  or other buffer gases with low liquefaction temperature due to its high liquefaction temperature (*i.e.*,  $-4.7^\circ\text{C}$ ). In addition, the toxicity of the  $C_3F_7CN/CO_2$  gas mixture with  $C_3F_7CN$  volume fraction below 10% is lower than that of pure  $SF_6$ . Thus, the former is harmless to humans.<sup>8</sup> These physical and chemical properties indicate that  $C_3F_7CN$  is excellent in terms of environmental protection, insulation and safety, and has immense potential to replace  $SF_6$ .

In the past two years, many scholars have proven that the  $C_3F_7CN/CO_2$  gas mixture has excellent insulation and arc extinguishing performance through numerous tests.<sup>3,7-10</sup> For engineering applications, a gas insulated line (GIL) with a rated voltage of 420 kV and a current transformer (CT) with a rated voltage of 245 kV using the  $C_3F_7CN/CO_2$  gas mixture as insulating medium were tested in 2015.<sup>3,8</sup> In addition, the investigation of the decomposition properties of a gas-insulating medium is an important component to comprehensively evaluate its performance. On the one hand, the insulation defects

<sup>a</sup>School of Electrical Engineering, Wuhan University, BaYi Street No. 299, Wuhan 430072, Hubei Province, China. E-mail: xiaosongxs@gmail.com; Tel: +86 18986238962

<sup>b</sup>Electric Power Research Institute, China Southern Power Grid, Guangzhou 510623, China

† Electronic supplementary information (ESI) available. See DOI: 10.1039/c7ra09959b

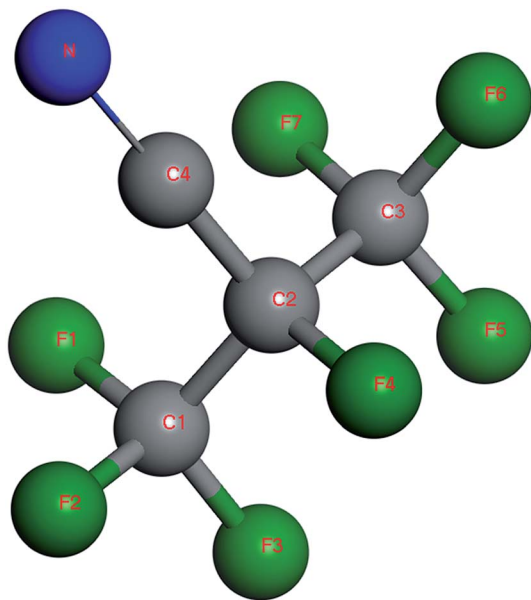


Fig. 1 Molecule structure of  $C_3F_7CN$ .

caused by aging under long-term operating conditions in electrical equipment will lead to partial discharge (PD) or flashover and is accompanied by the decomposition of the insulating medium. The local overheating fault can also lead to the decomposition of the insulating medium. On the other hand, the decomposition characteristics of the insulating medium are closely related to its self-recovery characteristics and arc-extinguishing properties.

At present, researches on the decomposition characteristics of  $C_3F_7CN$  have achieved noteworthy results. Kieffel *et al.* investigated the pyrolysis characteristics of the  $C_3F_7CN/CO_2$  gas mixture. They found the initial decomposition temperature of  $C_3F_7CN$  was 650 °C, thereby mainly producing decomposition

products, such as CO,  $CF_3CN$ , and  $C_2F_5CN$ .<sup>8</sup> Andersen *et al.* investigated the atmospheric chemistry of  $C_3F_7CN$  and evaluated its environmental effects based on density functional theory and infrared spectroscopy.<sup>11</sup> Our team has explored the decomposition mechanism of  $C_3F_7CN$  in the presence of trace water impurity through quantum chemical calculation. The ionization parameters of  $C_3F_7CN$  and various decomposition products were analyzed from the perspective of molecular structure, thereby providing a theoretical reference for the further study of the  $C_3F_7CN$  decomposition characteristics.<sup>12</sup>

At present, only a few studies have been conducted on the decomposition characteristics of the  $C_3F_7CN/CO_2$  gas mixture. Our previous studies on the decomposition mechanism of  $C_3F_7CN$  were from the perspective of individual molecule and did not consider the decomposition process in multi-molecular and gas mixture systems. In this paper, we constructed the multi-molecular and  $C_3F_7CN/CO_2$  gas mixture model to study the decomposition process of  $C_3F_7CN$  using the reactive force field molecular dynamics (ReaxFF-MD) method and density functional theory (DFT). The decomposition paths, reaction enthalpy, and products distribution of the  $C_3F_7CN$  gas mixture at different temperatures were firstly investigated. Relevant results provide guidance for further exploration on electrical properties and practical engineering application of  $C_3F_7CN$  gas mixture.

## 2 Theoretical methods and computational details

### 2.1 ReaxFF-MD simulation details

ReaxFF is based on bond order to describe the dissociation and formation of covalent bonds at the atomic level<sup>13</sup> and is a beneficial tool for studying chemical reactions and predicting the performance of new materials. During the past more than ten years, ReaxFF has been used to treat a variety of elements

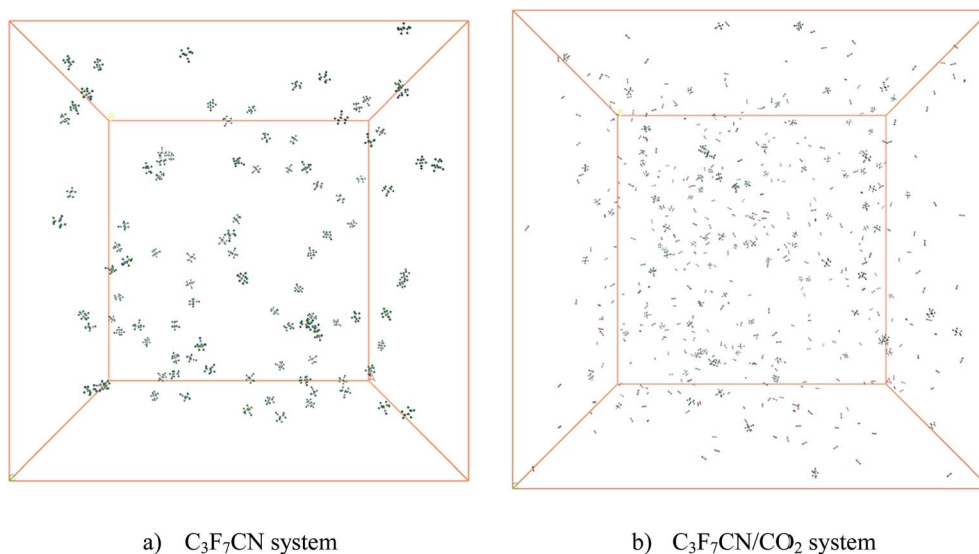


Fig. 2 Configurations of the  $C_3F_7CN$  and  $C_3F_7CN/CO_2$  systems.



and multifunctional systems and is suitable for describing polyatomic systems.<sup>14–16</sup> The energy expression of ReaxFF is presented as follows:

$$E_{\text{system}} = E_{\text{bond}} + E_{\text{over}} + E_{\text{under}} + E_{\text{val}} + E_{\text{pen}} + E_{\text{tors}} + E_{\text{conj}} + E_{\text{vdWaaals}} + E_{\text{Coulomb}}, \quad (1)$$

where  $E_{\text{bond}}$  corresponds to bond energy;  $E_{\text{over}}$  and  $E_{\text{under}}$  denote the over and under coordinated atoms, respectively, in the energy contribution;  $E_{\text{val}}$ ,  $E_{\text{pen}}$ ,  $E_{\text{tors}}$ ,  $E_{\text{conj}}$ ,  $E_{\text{vdWaaals}}$ , and  $E_{\text{Coulomb}}$  represent the valence angle term, penalty energy, torsion energy, conjugation effects to energy, nonbonded van der Waals interaction, and Coulomb interaction, respectively.

Two periodic cubic boxes were built to explore the decomposition of  $\text{C}_3\text{F}_7\text{CN}$  and the  $\text{C}_3\text{F}_7\text{CN}/\text{CO}_2$  gas mixture (see Fig. 2). The  $\text{C}_3\text{F}_7\text{CN}$  system contains 100  $\text{C}_3\text{F}_7\text{CN}$  molecules with a density of  $0.00811 \text{ g cm}^{-3}$ . The length of the box is  $159 \text{ \AA}$ . At present, many scholars have tested the insulation characteristics of  $\text{C}_3\text{F}_7\text{CN}/\text{CO}_2$  mixture and found that mixtures with 20%  $\text{C}_3\text{F}_7\text{CN}$  displayed dielectric strengths comparable to  $\text{SF}_6$ .<sup>4,7</sup> In order to reveal the decomposition properties of mixtures in this scale, we built the  $\text{C}_3\text{F}_7\text{CN}/\text{CO}_2$  system which contains 100  $\text{C}_3\text{F}_7\text{CN}$  molecules and 400  $\text{CO}_2$  molecules with a density of  $0.00351 \text{ g cm}^{-3}$ . The length of the box is  $260 \text{ \AA}$ . The initial density corresponds to the actual density of  $\text{C}_3\text{F}_7\text{CN}$  under  $25^\circ\text{C}$  and  $0.1 \text{ Mpa}$ . The system was minimized with the NVE ensemble for 5 ps at 5 K and equilibrated with the NVT ensemble thereafter for 10 ps at 1000 K using a time step of 0.1 fs.<sup>16</sup> The NVT simulations were then conducted at different temperatures for 1000 ps to explore the decomposition process of  $\text{C}_3\text{F}_7\text{CN}$  and  $\text{C}_3\text{F}_7\text{CN}/\text{CO}_2$  gas mixture. The temperature was controlled by the method of a Berendsen thermostat with a 0.1 ps damping constant.<sup>17</sup> All the ReaxFF-MD simulations in this paper were performed based on the ReaxFF module of ADF (Amsterdam Density Functional).<sup>18</sup>

## 2.2 DFT calculation details

The first principle of calculations based on the density functional theory (DFT) was performed to obtain the precise dissociation energy of  $\text{C}_3\text{F}_7\text{CN}$  at different temperatures. This theory is widely used in the study of chemical reaction mechanisms, and can describe any given chemical system with high accuracy.<sup>19–21</sup>

The spin unrestricted DFT calculation in the current study was performed based on the Dmol 3 module of the Materials studio 8.0. The meta-generalized approximation (mGGA) method treated by M06L functions is used to describe the exchange-correlation energy. This local density functional does well for predicting geometries and vibrational frequencies and gives great performance for a combination of main-group thermochemistry and thermochemical kinetics.<sup>22,23</sup> The double numerical atomic orbital augmented by d-polarization (DNP) is used as the basis set. Geometry optimizations were performed with the following convergence parameters: (1) energy convergence tolerance of  $1.0 \times 10^{-5} \text{ Ha}$ , (2) maximum force of  $0.002 \text{ Ha \AA}^{-1}$ , and (3) maximum displacement of  $0.005 \text{ \AA}$ . It should be pointed that spin contamination (unrestricted

DFT is much less affected by it than unrestricted Hartree–Fock theory<sup>24</sup>) and wave function instability may occur in spin unrestricted calculation. The self-consistent-field (SCF) solution stability is checked to ensure the accuracy of calculation results.

The enthalpy correction is presented as follows to obtain the precise energy of the system at a given temperature:<sup>25</sup>

$$\Delta E = \sum(E_{\text{product}} + \Delta E_{\text{product}}) - \sum(E_{\text{reactant}} + \Delta E_{\text{reactant}}), \quad (2)$$

where  $E_{\text{product}}$  and  $E_{\text{reactant}}$  correspond to the energy of the product and reactant, respectively, at 0 K and  $\Delta E_{\text{product}}$  and  $\Delta E_{\text{reactant}}$  correspond to the correcting values of the enthalpy of product and reactant, respectively, at a given temperature.

## 3 Results and discussion

### 3.1 Decomposition of the pure $\text{C}_3\text{F}_7\text{CN}$

**3.1.1 Decomposition process and main reaction paths.** The three main types of discharges in electrical equipment are the corona (partial discharge), arc, and spark discharges, wherein the corona and arc discharges are the most common.<sup>26</sup> The maximum temperature in the central region of the corona discharge is in the range of 700–1200 K and the highest temperature in the arc discharge region can reach 12 000 K.<sup>26–28</sup> The current study analyzed the decomposition mechanism of  $\text{C}_3\text{F}_7\text{CN}$  and its gas mixture at different temperatures to clarify the particle composition and product change. It should be noted that the time scale of ReaxFF MD simulation is normally limited to several dozens of nanoseconds due to the computational cost.<sup>28,29</sup> Hence, we enhance the temperatures to accelerate the simulation process to allow reactions can be observed.

First, the multi-molecular ReaxFF molecular dynamic simulations of  $\text{C}_3\text{F}_7\text{CN}$  were performed and demonstrated that the  $\text{C}_3\text{F}_7\text{CN}$  molecule began to decompose at 1900 K. Fig. 3 shows the time evolution of the major species of the  $\text{C}_3\text{F}_7\text{CN}$  decomposition at 1900 K. Table 1 shows the generation time of the major species and corresponding decomposition pathways. At 1900 K, the  $\text{C}_3\text{F}_7\text{CN}$  decomposition mainly produces free radicals, such as  $\text{CF}_3$ ,  $\text{C}_3\text{F}_7$ ,  $\text{CN}$ ,  $\text{CNF}$ ,  $\text{CF}_2$ ,  $\text{CF}$ ,  $\text{CF}_3\text{CFCN}(\text{C}_3\text{NF}_4)$ , and  $\text{F}$ . It is important to note that some free radicals, such as

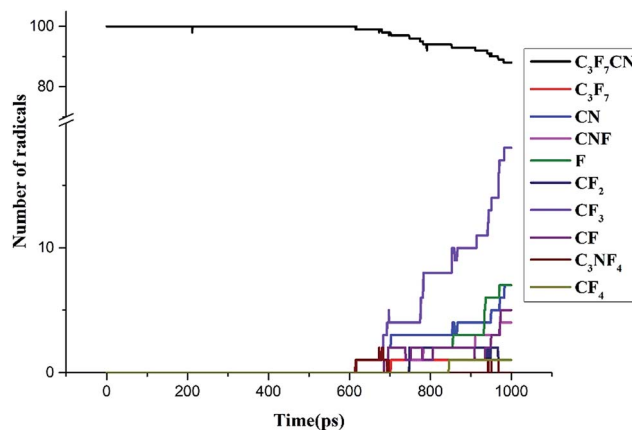


Fig. 3 Time evolution of the major species at 1900 K.



**Table 1** Generation time of the major species and corresponding decomposition pathways

Major species	Generation time (ps)	Reaction		$\Delta E^a$ (kcal mol <sup>-1</sup> )
C <sub>3</sub> NF <sub>4</sub> , CF <sub>3</sub>	615	A	C <sub>3</sub> F <sub>7</sub> CN → CF <sub>3</sub> + CF <sub>3</sub> CFCN	72.67
C <sub>3</sub> F <sub>7</sub>	702.5	B	C <sub>3</sub> F <sub>7</sub> CN → C <sub>3</sub> F <sub>7</sub> + CN	101.33
C <sub>4</sub> F <sub>6</sub> N	—	C	C <sub>3</sub> F <sub>7</sub> CN → (CF <sub>3</sub> ) <sub>2</sub> CCN + F	89.17
CN, CF	685.625	D	CF <sub>3</sub> CFCN → CF <sub>3</sub> + CF + CN	174.66
CF <sub>2</sub> , F	748.125	E	CF <sub>3</sub> → CF <sub>2</sub> + F	79.04
CNF	748.125	F	CN + F → CNF	−118.48
CF <sub>4</sub>	845.625	G	CF <sub>3</sub> + F → CF <sub>4</sub>	−107.64
C	—	H	CF → C + F	121.23

<sup>a</sup>  $T = 1900$  K, at mGGA-M06L level with ZPE and enthalpy corrections.

CN, are harmful free radicals and could produce toxic molecules. The content and toxicity of the decomposition products of C<sub>3</sub>F<sub>7</sub>CN need further test study before engineering application.

C<sub>3</sub>F<sub>7</sub>CN began to decompose at 615 ps, thereby producing CF<sub>3</sub>CFCN and CF<sub>3</sub>. This reaction path is required to absorb 72.67 kcal mol<sup>-1</sup>. Another decomposing path began at 702.5 ps, thereby producing C<sub>3</sub>F<sub>7</sub> and CN and needs to absorb 101.33 kcal mol<sup>-1</sup>. In addition, the decomposition of CF<sub>3</sub>CFCN is at 685.625 ps, thereby generating CF<sub>3</sub>, CF, and CN. CF<sub>3</sub> can further decompose to CF<sub>2</sub> and F by absorbing 79.04 kcal mol<sup>-1</sup>, CF can further decompose to C and F by absorbing 121.23 kcal mol<sup>-1</sup>. CF<sub>4</sub> is one of the stable decomposition products, which is formed by CF<sub>3</sub> and F and releases -107.64 kcal mol<sup>-1</sup>. In addition, the DFT calculation results show that the energy required for path A is lower than that for path B, which means that path A is more likely to occur than path B. And the ReaxFF-MD results show that the number of generated CF<sub>3</sub> increases rapidly during 700–1000 ps, which indicates the results of ReaxFF are consistent with DFT calculations and the performance of ReaxFF is reliable.

### 3.1.2 Effect of temperature on the decomposition process.

To further analyze the influence of temperature on the

decomposition process of C<sub>3</sub>F<sub>7</sub>CN, the molecular dynamic simulation of the C<sub>3</sub>F<sub>7</sub>CN system was performed at five temperature zones, that is, 1900 K, 2000 K, 2100 K, 2200 K, and 2400 K, for a total simulation time of 1000 ps.

Fig. 4 shows the time evolution of the potential energy between 1900 K and 2400 K. The potential energy of the system increases during the reaction process at different temperatures,

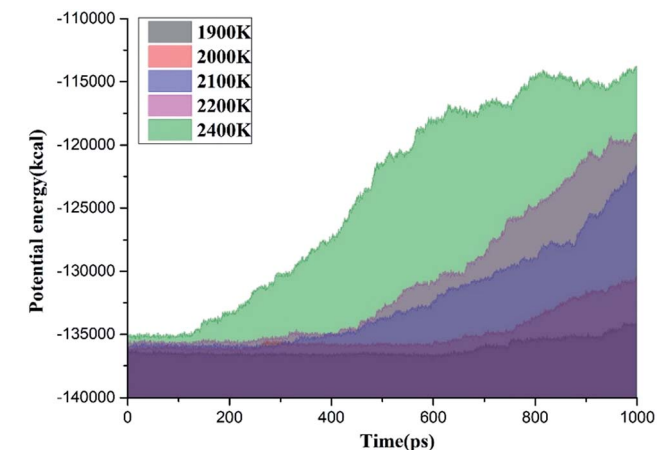
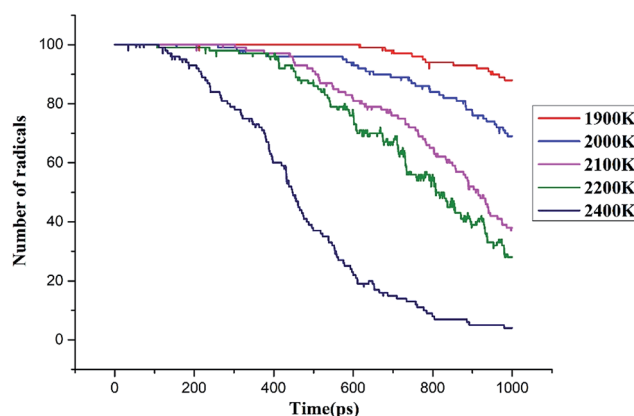


Fig. 5 Time evolution of the C<sub>3</sub>F<sub>7</sub>CN molecules decomposition when temperature is increased from 1900 to 2400 K (C<sub>3</sub>F<sub>7</sub>CN system).

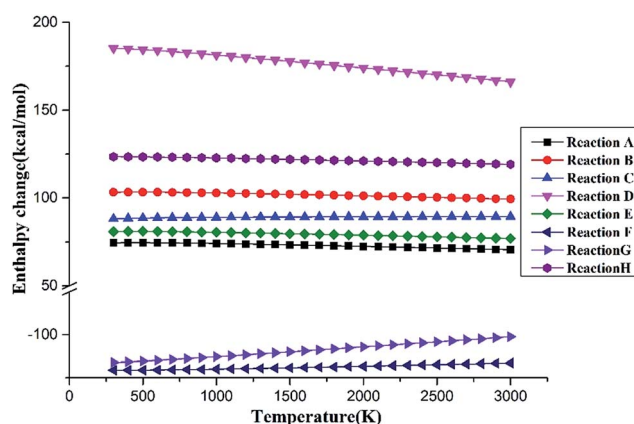


Fig. 4 Time evolution of the potential energy between 1900 K and 2400 K (C<sub>3</sub>F<sub>7</sub>CN system).

Fig. 6 Enthalpy change of the reaction pathways from 300 K to 3000 K.





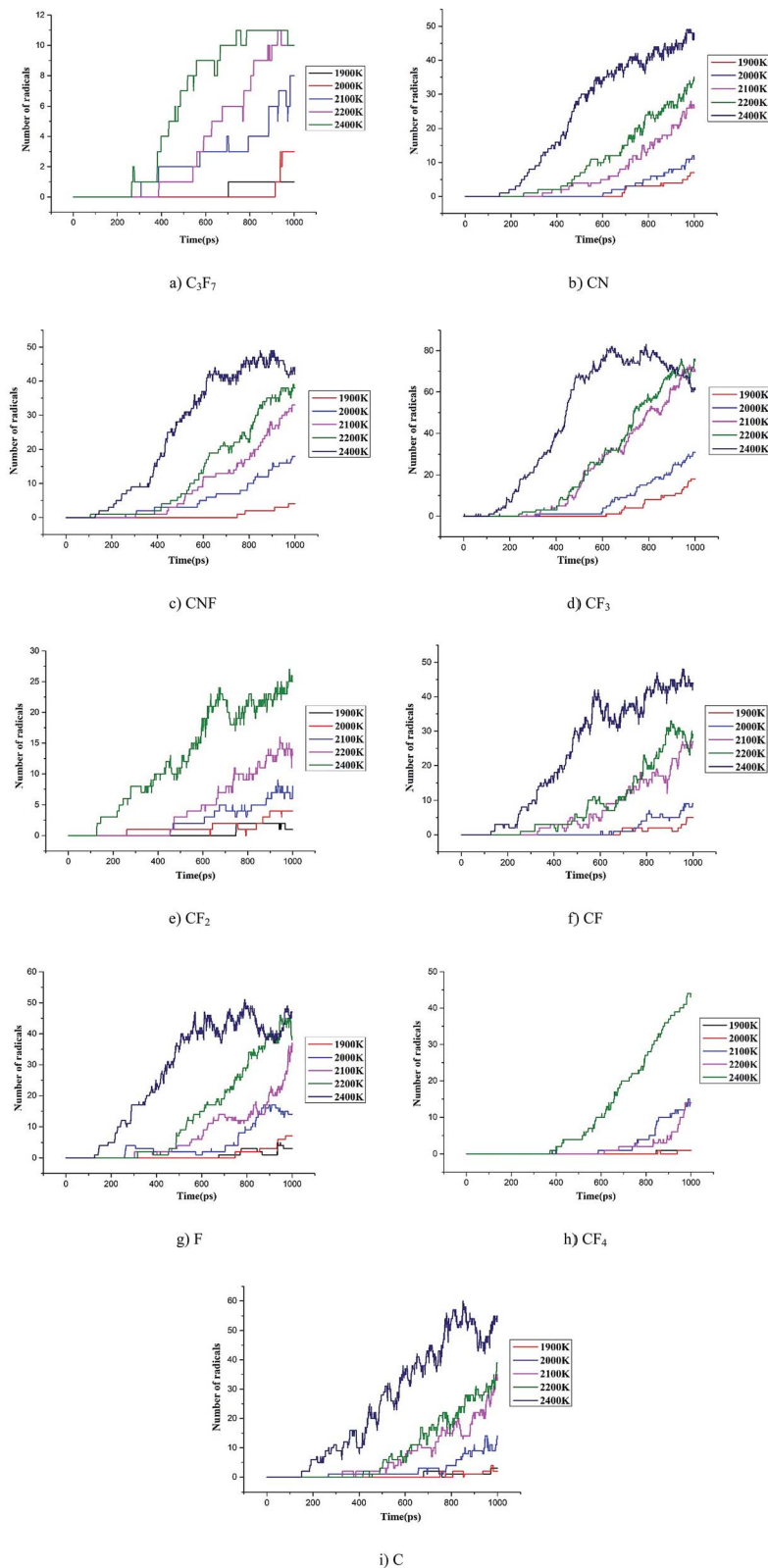


Fig. 7 Time evolution of the major species between 1900 K and 2400 K ( $C_3F_7CN$  system).

thereby indicating that the entire decomposition process of  $C_3F_7CN$  needs to absorb energy. The growth rate of the potential energy is evidently accelerated with the increase of temperature,

indicating that the increase of the ambient temperature will lead to the accelerated decomposition of  $C_3F_7CN$ . When the ambient temperature reaches 2400 K, the growth rate of the



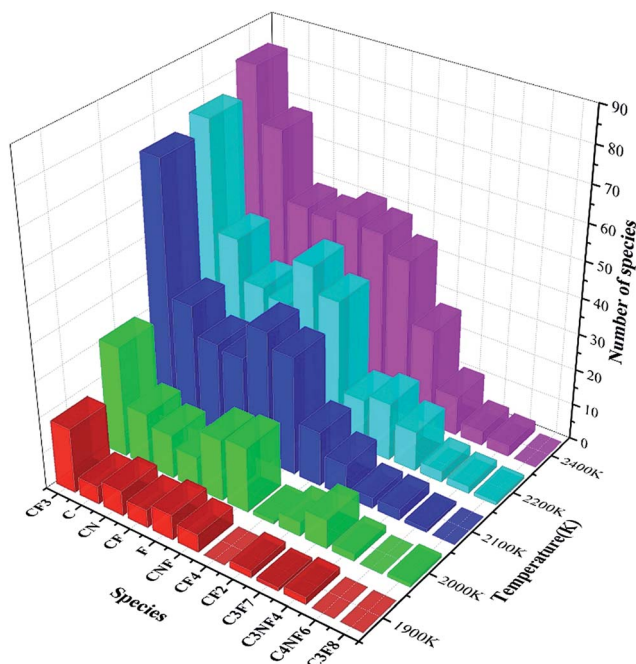


Fig. 8 Number of produced species in  $C_3F_7CN$  at different temperatures.

potential energy in the time range of 125 ps to 600 ps is significantly higher than that of 600–1000 ps. This result indicates that the reactions in the system before 600 ps are mainly absorbed energy. Moreover, exothermic reactions may occur in the system after 600 ps, thereby leading to the considerably gradual growth of the overall potential energy.

Fig. 5 illustrates the time evolution of the  $C_3F_7CN$  molecules between 1900 K and 2400 K. The decomposition rate and quantity of the  $C_3F_7CN$  molecules are evidently accelerated with the increase of temperature. For example, only 8  $C_3F_7CN$  molecules decomposed at 1900 K, whereas 96  $C_3F_7CN$  molecules decomposed at 2400 K at the end of the molecular dynamic simulation.

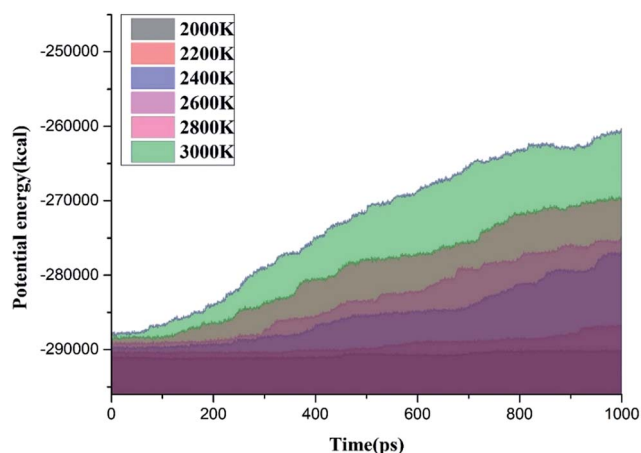


Fig. 9 Time evolution of the potential energy between 2000 K and 3000 K ( $C_3F_7CN/CO_2$  system).

To further analyze the effect of temperature on the decomposition of  $C_3F_7CN$ , the enthalpy of the main reaction paths in the temperature range of 300–3000 K is calculated based on DFT (see Fig. 6). As the temperature increases, the reaction enthalpy of paths A, B, D, and E decreases, that is, the temperature increase is favorable for the reaction progress. The enthalpy change of path D is the most evident, thereby indicating that the increase of temperature has a significant effect on the decomposition of  $CF_3CFCN$ . The reaction enthalpy change of paths C and H is not significantly with increasing temperature. Paths F and G are exothermic reaction processes and the energy released decreases as the temperature increases.

**3.1.3 Intermediates and main products.** Fig. 7 illustrates the time evolution of the major species of  $C_3F_7CN$  decomposition over the temperature range from 1900 K to 2400 K. Fig. 8 shows the maximum number of produced species. The statistical results in Fig. 7 shows that the amount of  $C_3F_7$ , CN, CNF,  $CF_3$ ,  $CF_2$ , CF,  $CF_3CFCN(C_3NF_4)$ , F, and other free radicals and  $CF_4$  produced by the decomposition of  $C_3F_7CN$  increased with the increase of temperature.

The statistical results in Fig. 8 show that the content of  $CF_3$  at each temperature is the highest among all the products, while the contents of  $CF_2$ , CN, CNF, and F are similar. The contents of  $C_3F_7$ ,  $C_3NF_4$ , and  $C_4NF_6$  are lower compared with those of other products.  $C_4NF_6$  is generated by the dissociation of the F atom in the  $C_3F_7CN$  molecule from the central C atom (C2 atom as shown in Fig. 1), thereby requiring the absorption of  $89.17 \text{ kcal mol}^{-1}$ . In addition, a few small stable molecules, such as  $CF_4$  and  $C_3F_8$ , are found during the simulation. The generation rate of  $CF_4$  in the time range of 600–1000 ps at 2400 K increased and the amount of  $CF_3$  and F during the time range reduced (as shown in Fig. 7). Given that the generation path of  $CF_4$  (path G in Table 1) is exothermic, the gradual growth of the overall potential energy of the system is actually due to the large amount of  $CF_4$  produced.

### 3.2 Decomposition of the $C_3F_7CN/CO_2$ mixture

#### 3.2.1 Effect of temperature on the decomposition process.

In order to obtain the decomposition properties of the insulating medium in a practical application condition, the

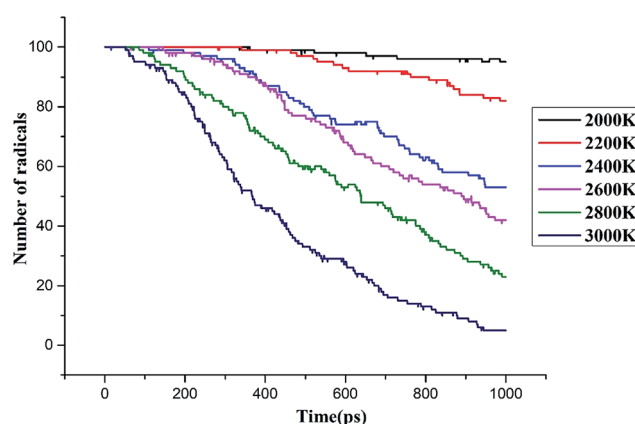


Fig. 10 Time evolution of the  $C_3F_7CN$  molecules decomposition when temperature is increased from 2000 to 3000 K ( $C_3F_7CN/CO_2$  system).



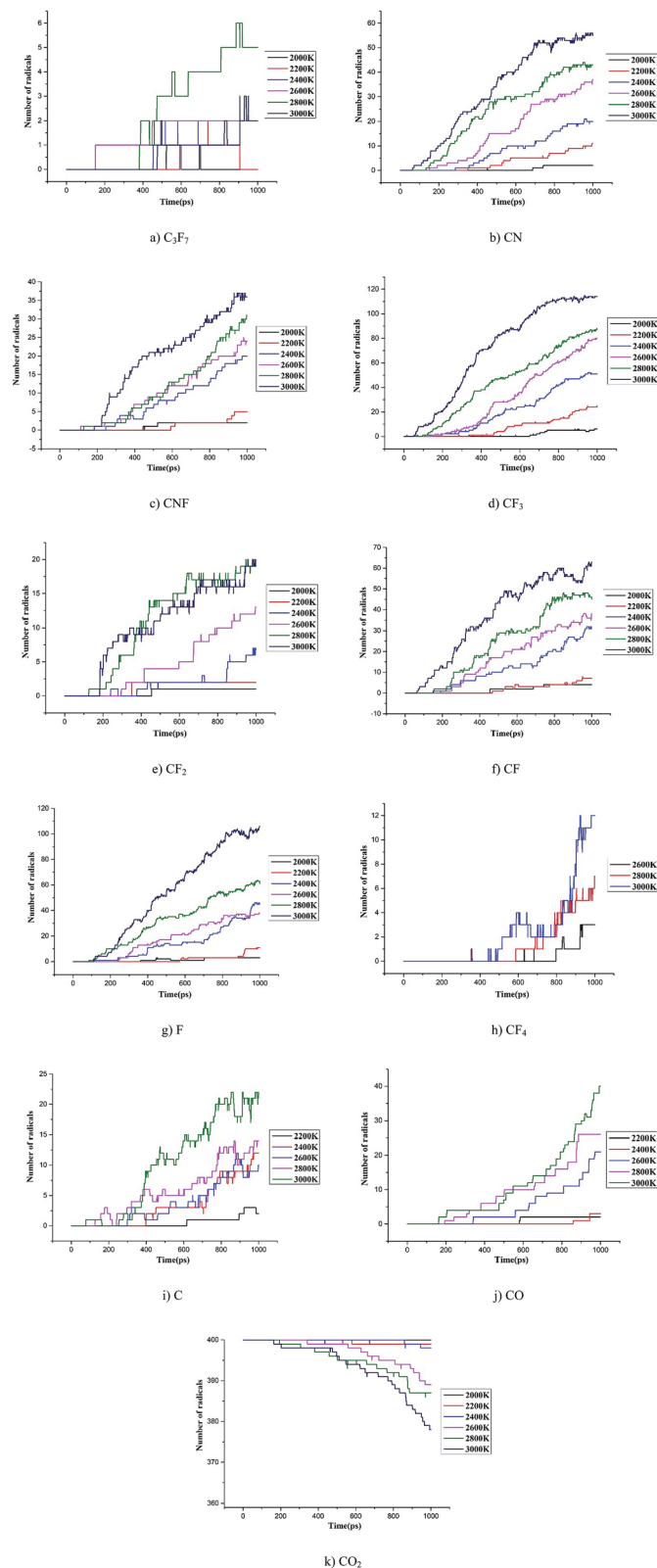


Fig. 11 Time evolution of the major species between 2000 K and 3000 K ( $C_3F_7CN/CO_2$  system).

decomposition characteristics of  $C_3F_7CN/CO_2$  gas mixture over the temperature range from 2000 K to 3000 K were discussed. Fig. 9 shows the time evolution of the potential energy of the

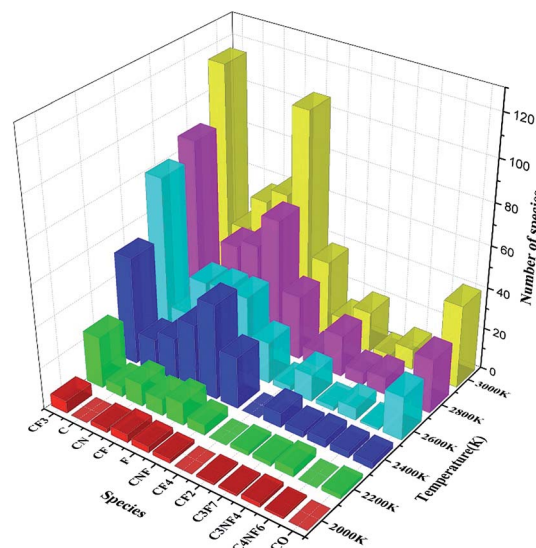


Fig. 12 Number of produced species in  $C_3F_7CN/CO_2$  at different temperatures.

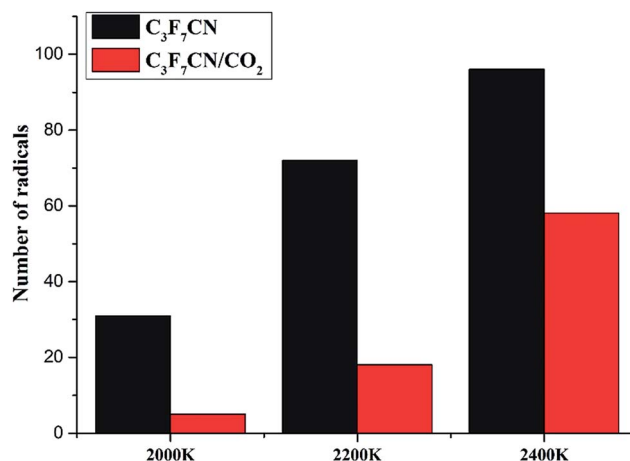


Fig. 13 Final decomposition amount of  $C_3F_7CN$  at different temperatures.

$C_3F_7CN/CO_2$  gas mixture system. Fig. 10 provides the decomposition amount of  $C_3F_7CN$ .

The potential energy of the system shows an increasing trend in the range of 2200–3000 K. When the ambient temperature is above 2400 K, the potential energy of the system increases. When the ambient temperature is 2000 K, the potential energy of the system does not change substantially, thereby exhibiting a relationship with the decomposition degree when  $C_3F_7CN$  is low. The decomposition rate of  $C_3F_7CN$  is accelerated with the increase of temperature, thereby showing consistency with the conclusion of the pure  $C_3F_7CN$  system.

**3.2.2 Intermediates and main products.** Fig. 11 describes the time evolution of the major decomposition species of  $C_3F_7CN$  over the temperature range from 2000 K to 3000 K. Fig. 12 presents the maximum number of produced species.



Table 2 Final amount of the decomposition products at different temperatures

Major species	Temperature					
	2000 K		2200 K		2400 K	
	C <sub>3</sub> F <sub>7</sub> CN	C <sub>3</sub> F <sub>7</sub> CN/CO <sub>2</sub>	C <sub>3</sub> F <sub>7</sub> CN	C <sub>3</sub> F <sub>7</sub> CN/CO <sub>2</sub>	C <sub>3</sub> F <sub>7</sub> CN	C <sub>3</sub> F <sub>7</sub> CN/CO <sub>2</sub>
C <sub>3</sub> F <sub>7</sub>	8	1	11	2	11	3
CF <sub>3</sub>	31	6	76	25	83	52
CF <sub>2</sub>	4	1	16	2	27	7
CF	9	4	33	8	48	32
CN	12	2	35	11	49	21
CNF	18	2	39	5	49	25
F	17	3	46	11	51	46
C <sub>3</sub> NF <sub>4</sub>	2	2	3	4	4	4
C <sub>4</sub> NF <sub>6</sub>	0	1	2	0	3	3
CF <sub>4</sub>	1	0	14	0	44	0
C	15	0	46	5	68	16

Similar to the pure C<sub>3</sub>F<sub>7</sub>CN system, the content of the major decomposition products shows an increasing trend with the increase of temperature. The content of CF<sub>3</sub> in the products is the highest at each temperature. When the temperature is below 2800 K, the yields of CN, CNF, CF, and F are similar. When the temperature is above 2800 K, the content of F in the system increases. A new decomposition of products, namely, CO, is produced due to the addition of CO<sub>2</sub>. The decomposition of CO<sub>2</sub> accelerated at temperatures over 2600 K and 40 molecules of CO are produced at 3000 K. In the C<sub>3</sub>F<sub>7</sub>CN/CO<sub>2</sub> system, the yield of CF<sub>4</sub> reduces. Only 12 CF<sub>4</sub> molecules were produced at 3000 K at the end of the simulation, which is lower than that of the pure C<sub>3</sub>F<sub>7</sub>CN system. In addition, the generation rate of CF<sub>3</sub> and F after 800 ps at 3000 K slowed down, which is related to the formation of CF<sub>4</sub>.

**3.2.3 Effect of CO<sub>2</sub> on the decomposition process.** Fig. 13 shows the final decomposition amount of C<sub>3</sub>F<sub>7</sub>CN in C<sub>3</sub>F<sub>7</sub>CN and C<sub>3</sub>F<sub>7</sub>CN/CO<sub>2</sub> system at the same temperature. The decomposition amount of C<sub>3</sub>F<sub>7</sub>CN in the C<sub>3</sub>F<sub>7</sub>CN/CO<sub>2</sub> gas mixture system is lower than that in the pure C<sub>3</sub>F<sub>7</sub>CN system at the same temperature. For example, the decomposition amount in the pure C<sub>3</sub>F<sub>7</sub>CN system is 96 at 2400 K, whereas that of the C<sub>3</sub>F<sub>7</sub>CN/CO<sub>2</sub> gas mixture system is 58. The addition of the buffer gas CO<sub>2</sub> can effectively inhibit the decomposition of C<sub>3</sub>F<sub>7</sub>CN.

Table 2 shows that the final amount of the decomposition products in the C<sub>3</sub>F<sub>7</sub>CN/CO<sub>2</sub> gas mixture system is lower than that in the pure C<sub>3</sub>F<sub>7</sub>CN system at the same temperature. Moreover, the addition of CO<sub>2</sub> inhibits the formation of CF<sub>4</sub> and C, thereby making it difficult for the system to precipitate carbon and produce products with relatively poor insulation properties. This result is beneficial to protect the insulation properties of the system.

Therefore, the C<sub>3</sub>F<sub>7</sub>CN/CO<sub>2</sub> gas mixture is relatively suitable for using as a gas-insulated medium relative to pure C<sub>3</sub>F<sub>7</sub>CN. The mechanism of the action of CO<sub>2</sub> over C<sub>3</sub>F<sub>7</sub>CN to avoid its decomposition process in function of temperature needs further study.

## 4 Conclusion

This study analyzed the decomposition characteristics of C<sub>3</sub>F<sub>7</sub>CN and its gas mixture based on ReaxFF-MD method and density functional theory. The main decomposition pathways, reaction enthalpy, and the composition of the main decomposition products of C<sub>3</sub>F<sub>7</sub>CN at different temperatures were revealed. The decomposition characteristics of C<sub>3</sub>F<sub>7</sub>CN and C<sub>3</sub>F<sub>7</sub>CN/CO<sub>2</sub> gas mixture were compared and analyzed.

The decomposition of C<sub>3</sub>F<sub>7</sub>CN mainly produces CF<sub>3</sub>, C<sub>3</sub>F<sub>7</sub>, CN, CNF, CF<sub>2</sub>, CF, F, and other free radicals and a few molecular products, such as CF<sub>4</sub> and C<sub>3</sub>F<sub>8</sub>. The decomposition rate of C<sub>3</sub>F<sub>7</sub>CN and generation rate of the products increase with the increase of ambient temperature. The C<sub>3</sub>F<sub>7</sub>CN/CO<sub>2</sub> gas mixture has more excellent decomposition characteristics than that of pure C<sub>3</sub>F<sub>7</sub>CN at the same condition, which is relatively suitable for use as a gas-insulated medium in electrical equipment.

## Conflicts of interest

There are no conflicts to declare.

## Acknowledgements

The current work is supported by the science and technology project of China Southern Power Grid (No. CSGTRC-K163010)

## References

- 1 A. Beroual and A. Haddad, Recent Advances in the Quest for a New Insulation Gas with a Low Impact on the Environment to Replace Sulfur Hexafluoride (SF<sub>6</sub>) Gas in High-Voltage Power Network Applications, *Energies*, 2017, **10**(8), 1216.
- 2 X. Zhang, Y. Li, S. Xiao, *et al.*, Decomposition mechanism of C<sub>5</sub>F<sub>10</sub>O: An environmentally friendly insulation medium, *Environ. Sci. Technol.*, 2017, **51**(17), 10127–10136.
- 3 J. Reilly, R. Prinn, J. Harnisch, *et al.*, Multi-gas assessment of the Kyoto Protocol, *Nature*, 1999, **401**(6753), 549.





- 4 Y. Kieffel, T. Irwin, P. Ponchon, *et al.*, Green Gas to Replace SF<sub>6</sub> in Electrical Grids, *IEEE Power and Energy Magazine*, 2016, **14**(2), 32–39.
- 5 M. P. Sulbaek Andersen, M. Kyte, S. T. Andersen, *et al.*, Atmospheric Chemistry of (CF<sub>3</sub>)<sub>2</sub>CFCN: A Replacement Compound for the Most Potent Industrial Greenhouse Gas, SF<sub>6</sub>, *Environ. Sci. Technol.*, 2017, **51**(3), 1321–1329.
- 6 Z. Lv, D. Zhao and S. Xu, Facile synthesis of mesoporous melamine-formaldehyde spheres for carbon dioxide capture, *RSC Adv.*, 2016, **6**(64), 59619–59623.
- 7 J. G. Owens, Greenhouse gas emission reductions through use of a sustainable alternative to SF<sub>6</sub>, *IEEE Electrical Insulation Conference (EIC)*, Montréal, Canada, 2016, pp. 535–538.
- 8 Y. Kieffel, Characteristics of g3-an alternative to SF<sub>6</sub>, *IEEE International Conference on Dielectrics(ICD)*, Montpellier, France, 2016, vol. 2, pp. 880–884.
- 9 H. E. Nechmi, A. Beroual, A. Girodet, *et al.*, Fluoronitriles/CO<sub>2</sub> Gas Mixture as Promising Substitute to SF<sub>6</sub> for Insulation in High Voltage Applications, *IEEE Trans. Dielectr. Electr. Insul.*, 2016, **23**(5), 2587–2593.
- 10 C. Preve, R. Maladen and D. Piccoz, Method for validation of new eco-friendly insulating gases for medium voltage equipment, *IEEE International Conference on Dielectrics (ICD)*, Montpellier, France, 2016, vol. 1, pp. 235–240.
- 11 M. P. S. Andersen, M. Kyte, S. T. Andersen, C. J. Nielsen and O. J. Nielsen, Atmospheric Chemistry of (CF<sub>3</sub>)<sub>2</sub>CF–CN: A Replacement Compound for the Most Potent Industrial Greenhouse Gas, SF<sub>6</sub>, *Environ. Sci. Technol.*, 2017, **51**(3), 1321–1329.
- 12 X. Zhang, Y. Li, S. Xiao, *et al.*, Theoretical study of the decomposition mechanism of environmentally friendly insulating medium C<sub>3</sub>F<sub>7</sub>CN in the presence of H<sub>2</sub>O in a discharge, *J. Phys. D: Appl. Phys.*, 2017, **50**(32), 325201.
- 13 A. C. T. V. Duin, S. Dasgupta, F. Lorant, *et al.*, ReaxFF: A Reactive Force Field for Hydrocarbons, *J. Phys. Chem. A*, 2001, **105**(41), 9396–9409.
- 14 J. Zhang, Y. Si, C. Leng, *et al.*, Molecular dynamics simulation of Al–SiO<sub>2</sub> sandwich nanostructure melting and low-temperature energetic reaction behavior, *RSC Adv.*, 2016, **6**(64), 59313–59318.
- 15 S. Bhoi, T. Banerjee and K. Mohanty, Insights on the combustion and pyrolysis behavior of three different ranks of coals using reactive molecular dynamics simulation, *RSC Adv.*, 2016, **6**(4), 2559–2570.
- 16 D. Hong, L. Liu, Y. Huang, *et al.*, Chemical effect of H<sub>2</sub>O on CH<sub>4</sub> oxidation during combustion in O<sub>2</sub>/H<sub>2</sub>O environments, *Energy Fuels*, 2016, **30**(10), 8491–8498.
- 17 H. J. C. Berendsen, J. P. M. Postma, W. F. V. Gunsteren, *et al.*, Molecular dynamics with coupling to an external bath, *J. Chem. Phys.*, 1984, **81**(8), 3684–3690.
- 18 G. Te Velde, F. M. Bickelhaupt, E. J. Baerends, *et al.*, Chemistry with ADF, *J. Comput. Chem.*, 2001, **22**(9), 931–967.
- 19 T. C. Ngo, D. Q. Dao, M. T. Nguyen, *et al.*, A DFT analysis on the radical scavenging activity of oxygenated terpenoids present in the extract of the buds of *Cleistocalyx operculatus*, *RSC Adv.*, 2017, **7**(63), 39686–39698.
- 20 Q. Zhou, X. Su, W. Ju, *et al.*, Adsorption of H<sub>2</sub>S on graphane decorated with Fe, Co and Cu: a DFT study, *RSC Adv.*, 2017, **7**(50), 31457–31465.
- 21 P. Zhang, X. Hou, J. Mi, *et al.*, Curvature Effect of SiC Nanotubes and Sheet for CO<sub>2</sub> Capture and Reduction, *RSC Adv.*, 2014, **4**(90), 48994–48999.
- 22 Y. Zhao and D. G. Truhlar, The M06 suite of density functionals for main group thermochemistry, thermochemical kinetics, noncovalent interactions, excited states, and transition elements: two new functionals and systematic testing of four M06-class functionals and 12 other functionals, *Theoretical Chemistry Accounts: Theory, Computation, and Modeling*, 2008, **120**(1), 215–241.
- 23 Y. Zhao and D. G. Truhlar, A new local density functional for main-group thermochemistry, transition metal bonding, thermochemical kinetics, and noncovalent interactions, *J. Chem. Phys.*, 2006, **125**(19), 194101.
- 24 A. S. Menon and L. Radom, Consequences of spin contamination in unrestricted calculations on open-shell species: effect of Hartree-Fock and Møller-Plesset contributions in hybrid and double-hybrid density functional theory approaches, *J. Phys. Chem. A*, 2008, **112**(50), 13225–13230.
- 25 X. Zhang, S. Xiao, J. Zhang, *et al.*, Influence of humidity on the decomposition products and insulating characteristics of CF<sub>3</sub>I, *IEEE Trans. Dielectr. Electr. Insul.*, 2016, **23**(2), 819–828.
- 26 R. Ono and T. Oda, Measurement of gas temperature and OH density in the afterglow of pulsed positive corona discharge, *J. Phys. D: Appl. Phys.*, 2008, **41**(3), 035204.
- 27 Y. Fu, M. Rong, K. Yang, *et al.*, Calculated rate constants of the chemical reactions involving the main byproducts SO<sub>2</sub>F, SOF<sub>2</sub>, SO<sub>2</sub>F<sub>2</sub> of SF<sub>6</sub> decomposition in power equipment, *J. Phys. D: Appl. Phys.*, 2016, **49**(15), 155502.
- 28 H. Tanaka, D. Tanahashi, Y. Baba, *et al.*, Finite-difference time-domain simulation of partial discharges in a gas insulated switchgear, *High Voltage*, 2016, **1**(1), 52–56.
- 29 Z. Chen, W. Sun and L. Zhao, High-temperature and High-pressure Pyrolysis of Hexadecane: A Molecular Dynamic Simulation Based on Reactive Force Field (ReaxFF), *J. Phys. Chem. A*, 2017, **121**(10), 2069.

